SOUNDNESS DISCRIMINATION IN FERRITE DUCTILE IRONS THROUGH TENSILE DATA ANALYSIS

G. Angella
CNR-ICMATE, Via R. Cozzi 53, 20125 Milan, MI, Italy

M. Cova
SACMI, Via Salice Provinciale 17/A, 40026 Imola, BO, Italy

G. Bertuzzi
Petrovalves S.p.A., Viale Giuseppe Borri, 42, 21053 Castellanza, VA, Italy

F. Zanardi
Zanardi Fonderie S.p.A., Viale Nazionale 3, 37046 Minerbe, VR, Italy

https://doi.org/10.1007/s40962-020-00435-0

Abstract

Ferritic ductile iron (DI) GJS 400 and high-silicon strengthened ductile irons (HSSDIs) with 3.5 and 4.5 wt% of silicon contents were produced with different cooling rates, and the microstructures were analyzed to find the main microstructure parameters. The Y-blocks GJS 400 presented good nodularity, while the heavy section GJS 400 presented some graphite degeneracy with a lower nodularity. The 3.5 wt% HSSDI shown a good nodularity, while with increasing silicon content to 4.5 wt%, significant graphite degeneracy occurred with the appearance of chunky graphite. Samples were tensile tested and the tensile data were analyzed through the physical-based constitutive Voce equation, and the Voce parameters were plotted to produce a matrix assessment diagram (MAD). Y-blocks and heavy section GJS 400 data lied on two distinct lines in MAD, and they had, however, positive and negative intercepts which meant indeed two contradictory plastic behaviors. The intercept of the best fitting line of the GJS 400 Y-blocks data was positive and so consistent with the physical meaning of Voce equation, while the intercept of the best fitting line of the GJS 400 heavy section data was negative, which meant an unexpected opposite plastic behavior. Same behavior was reported for the investigated HSSDIs, resulting in positive intercept of the best fitting line in MAD for the 3.5 wt% HSSDI data and negative intercept for the 4.5 wt% HSSDI data. The uniform strain energy density (SED_U) that is the area below the tensile flow curve up to the uniform strain, i.e., the strain where necking begins, was also investigated. SED_U resulted to be almost constant for all the GJS 400 Y-blocks tensile flow curves and 3.5 wt% HSSDI, which was typical of a sound material, while in GJS 400 heavy section and 4.5 wt% HSSDI, SED_U changed significantly in a systematic way, indicating that metallurgical defects had affected the plastic behavior. So it was concluded that in the MAD the best fitting line of the tensile data with positive intercept was a possible indication of the material soundness, while the negative intercept was indication of defected material. The results suggested that the MAD analysis produced from tensile Voce parameters can be a useful and easy tool for industry not only to classify the production routes of DIs (Si content mainly and heat treatments), but also to identify possible microstructure poorness within a single DI grade.

Keywords: *ductile irons, Y-blocks, heavy sections, tensile properties, microstructure quality assessment*

Introduction

Process–microstructure–property relationships have always represented a key issue in the industrial production and

This paper is an invited submission to IJMC selected from presentations at the 2nd Carl Loper 2019 Cast Iron Symposium held September 30 to October 1, 2019, in Bilbao, Spain.

application of materials. Microstructure in ductile irons (DIs) may enclose defects and metallurgical discontinuities, like irregular morphology graphite, slag inclusions, shrinkages and gas holes, which may cause high variability in their mechanical properties. To minimize this variability, the integrity of DIs, that is, the absence of defects and metallurgical discontinuities, should be easily evaluated through procedures based on tensile testing[1,2] that represents the simplest mechanical examination.

A quality assessment procedure based on tensile testing should be capable both of classifying the different DI microstructures produced through different chemical compositions (mainly silicon content) and different production routes, and of giving indications of potential defects that may affect the mechanical properties of materials. Using the minimal tensile properties (yield stress, tensile stress and ductility) may be not sufficient, so, as the correlation between microstructure and tensile plastic behavior is our concern, dislocation dynamics should be considered through modeling tensile flow curves with dislocation-density-related constitutive equations that have physical bases and can give some deeper information on microstructure–property relationships. In References 3 and 4, a physical meaning of the differential form of the dislocation-density-related Voce equation was given. The Voce equation parameters are related to the microstructure characteristic features, and the plastic deformation micromechanisms, like dislocation density storage, and dislocation density decrease caused by dynamic recovery. Reference 5 shows that Voce equation described properly the strain hardening behaviors of a wide range of DI grades, like ferritic–pearlitic, pearlitic–ferritic isothermed DIs (IDIs) and austempered DIs (ADIs), while the empirical Hollomon-type equations failed.

A mathematical procedure based on modeling tensile flow curves through Voce equation has given promising results on both process–microstructure classification and integrity assessment of a wide number of different DI grades.[6,7] It is based on two diagrams: The first is the matrix assessment diagram (MAD) where the Voce equation parameters $1/\varepsilon_c$ versus Θ_o are plotted. In MAD, data from DIs with different chemical compositions and different production routes lied on specific lines, so the MAD approach was capable of identifying unambiguously different grades of DIs. The second is the integrity assessment diagram (IAD) consisting of the plot of the experimental elongations to rupture versus the theoretical uniform elongations (where necking occurs) calculated with the Voce formalism. IAD should be capable of identifying whether potential defects are present, as material rupture occurs prematurely before necking if defects are present, while it occurs beyond necking for sound materials. The procedure is based on the fundamental assumption that the defects do not affect the strain hardening behavior of DIs, which has been validated in IDI 800 produced through Y-block molds.[8] In the investigated IDI 800 samples, no metallurgical discontinuities were found and nodularity was excellent, since nodularity was about 90% for all samples. Even if significant differences in the elongations to ruptures in IAD were found, the strain hardening behaviors of the investigated IDI 800 samples were not affected. So it was concluded that single defects in the matrix should have affected only the elongations to rupture according to the fracture mechanics. No diffuse defects in IDIs 800 were present, or at least their nature and density were below a significant threshold and did not affect the flow curve shapes.

In DIs produced through heavy sections where the solidification rates are very slow, the nodule count decreases and nodule size increases, while graphite degenerates causing the decrease in nodularity and even the possible appearance of chunky graphite.[9,10] All of this leads to decreasing and scattering mechanical properties.[11,12] So in heavy sections, the sizes and the density of defects are expected to affect significantly the strain hardening behavior and the quality assessment procedure might need some corrections. High-silicon strengthened DIs (HSSDIs) with silicon content higher than 3.0 wt% presents fully ferritic microstructure with increased strength and moderate ductility reduction with respect to the conventional ferritic–pearlitic DI grades with similar strength.[13,14] However, for silicon content higher than 4.2 wt% and slow cooling rates, an abrupt decrease in ductility occurs, because of chemical ordering and graphite degeneration with possible chunky graphite.[15,16] Also in HSSDIs with silicon content of higher 4.2 wt% produced through slow rates, the strain hardening behavior is expected to be affected, and so, also this grade is a useful alloy to test the potentiality of the quality assessment procedure.

In the present paper, the comparison of the results of the analysis through the quality assessment procedure based on the matrix assessment diagram (MAD) within two different DI grades is reported. Conventional ferritic GJS 400 was produced through Y-blocks and heavy section, while ferritic 3.5 and 4.5 wt% HSSDIs were produced through 50- and 75-mm Y-blocks to experience different cooling rates. The investigation was focused on the capability of the quality assessment procedure to give indications of the integrity of the tested DIs, even if strain hardening behavior could be affected by metallurgical discontinuities or defects like in GJS 400 produced in heavy section and in 4.5 wt% HSSDIs produced with slow cooling rates.

Materials and Experimental

GJS 400 Microstructure

GJS 400 Y-Blocks

GJS 400 (C = 3.63 wt %, Si = 2.45, Mn = 0.13, Mg = 0.046, Cu = 0.133, Ni = 0.017, Cr = 0.023, P = 0.038,

S = 0.043, Fe = bal.) was produced in Zanardi Fonderie S.p.A. through four different mold geometries: a cylindrical Lynchburg mold with 25 mm diameter (the modified keel mold per ASTM A 536-84(2019)e1 Figure 4) and three different Y-block molds with increasing thickness 25, 50 and 75 mm complying on the standard ASTM A 536-84 including heavy sections. Scanning electron microscope (SEM) SU70 by Hitachi was used to observe the microstructure of GJS 400 produced in Y-blocks. An example of the microstructure of GJS 400 produced through 50-mm Y-block mold is shown in Figure 1, reporting nodular graphite in ferrite with some extent of pearlite (light areas). The microstructure presented a good nodularity and some area fraction of pearlite.

Nodule count (C_N), average graphite nodule diameter (S_N), nodularity (Nod.) and area fractions of pearlite (X_P) were measured by digital image analysis complying on ASTM E2567-16a, and data are reported in Table 1, where the parameters are the average of six samples for each solidification condition. In Lynchburg samples, there was no significant pearlite, while in the Y-blocks the pearlite area fractions spanned from about 3–4%. The pearlite formation was rationalized in terms of positive micro-segregations of Mn and negative micro-segregations of Si that formed during the solidification.[17]

GJS 400 Heavy Section

GJS 400 (C = 3.51 wt%, Si = 2.52, Mn = 0.19, Mg = 0.053, Cu = 0.098, Ni = 0.019, Cr = 0.032, P = 0.038, S = 0.065, Fe = bal.) was tested in SACMI S.p.A. through a heavy section of the weight of ~ 1050 kg with dimensions 1200 mm × 400 mm × 320 mm. Fourteen thermocouples were embedded in the middle of the 320 mm thickness of the section to measure the rates, and samples were core-drilled from the same 14 positions for machining tensile test specimens. Light microscopy (LM) was used to observe the microstructure of GJS 400 produced in heavy section. Detailed microstructure results and mechanical properties are reported in Reference 18. An example of the microstructure of GJS 400 produced through heavy section position F_Ext is reported in Figure 2. The size of the graphite is significantly larger than the one reported in Figure 1, and also, the morphology is very irregular, revealing a significant degeneracy of graphite, which is typical of heavy sections DIs.[19,20]

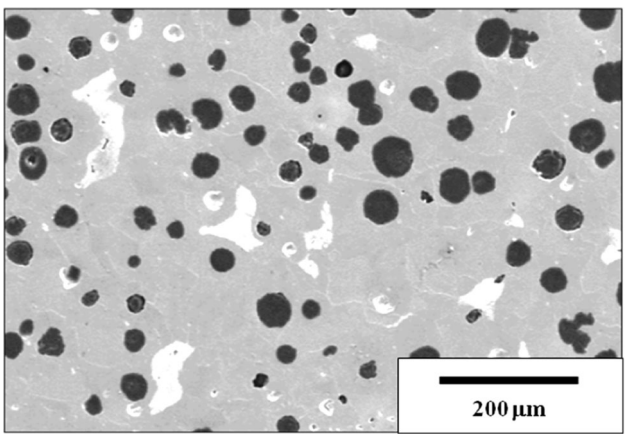

Figure 1. Secondary electron imaging (SEI) micrograph of GJS 400 produced through 50-mm Y-block mold.

Table 1. Microstructure Parameters of GJS 400 Produced Through Different Y-block and Lynchburg Molds

Mold	C_N (mm^{-2})	S_N (µm)	Nod. (%)	X_P (%)
Lynchburg	261.1	24.3	89.8	–
Y 25 mm	241.9	24.9	91.2	3.84
Y 50 mm	115.7	31.5	87.1	3.98
Y 75 mm	104.7	34.5	83.2	3.02

Nodule count (C_N), average diameter of the graphite nodules (S_N), nodularity (Nod.) and area fractions of pearlite (X_P) of seven selected positions were measured complying on ASTM E2567, and data are reported in Table 2.

HSSDI Microstructure

HSSDIs with silicon contents of about 3.5 wt% (C = 3.49 wt%, Si = 3.48, Mn = 0.11, Mg = 0.045, P = 0.028, S = 0.006, Fe = bal.) and about 4.5 wt% (C = 3.59 wt %, Si = 4.46, Mn = 0.15, Mg = 0.051, P = 0.035, S = 0.005, Fe = bal.) were produced in Zanardi Fonderie S.p.A. through 75 and 50-mm Y-block molds complying on the standard ASTM A 536-84. Examples of the microstructure of HSSDIs with about 3.5 and 4.5 wt% silicon contents are reported in Figures 3 and 4, respectively. Nodule count (C_N), average graphite nodule diameter (S_N) and nodularity (Nod.) measured by digital image analysis complying on

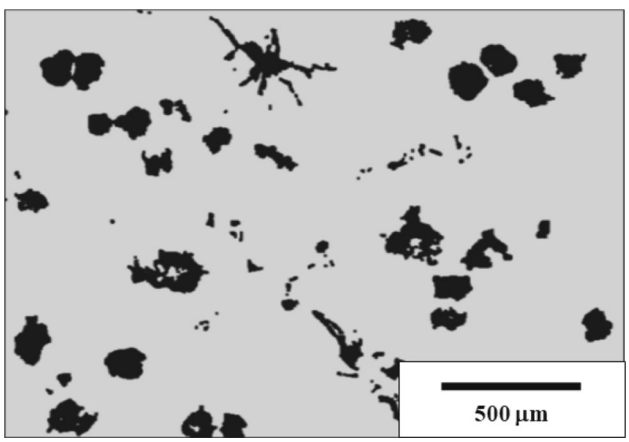

Figure 2. Light microscopy (LM) micrograph of GJS 400 produced through heavy section.

Table 2. Microstructure Parameters of GJS 400 Produced Through Heavy Section

Position	C_N (mm^{-2})	S_N (μm)	Nod. (%)	X_P (%)
A_Ext	32.1	55.6	65.8	< 3
C_Ext	52.2	46.0	75.9	< 3
D_Ext	33.2	59.5	73.8	< 3
D_Int	30.4	64.2	71.6	< 3
E_Int	27.8	62.1	53.2	< 3
F_Ext	29.9	57.6	70.2	< 3
F_Int	22.7	69.9	65.3	< 3

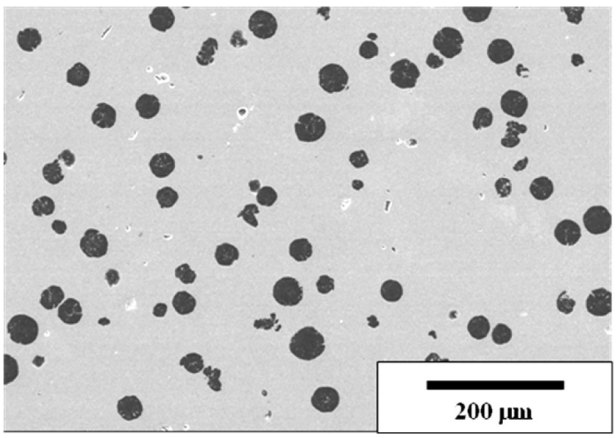

Figure 3. Secondary electron imaging (SEI) micrograph of 3.5 wt% HSSDI produced in 75-mm Y-block.

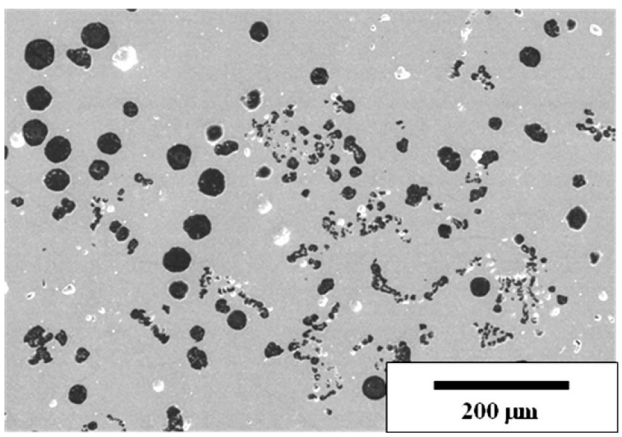

Figure 4. Secondary electron imaging (SEI) micrograph of 4.5 wt% HSSDI produced in 75-mm Y-block.

ASTM E2567-16a are reported in Table 3, where the parameters are the average of three samples for each solidification condition. No pearlite was found, and the nodularity was higher than 80% with 3.5 wt% of silicon content samples, while with increasing silicon content the nodularity was below 70% and the graphite presented some degeneracy with the appearance of chunky graphite, as

Table 3. Microstructure Parameters of HSSDIs with 3.5 and 4.5 wt% Silicon Content Produced Through 75- and 50-mm Y-Block Molds

Si wt%	Mold (mm)	C_N (mm^{-2})	S_N (μm)	Nod. (%)
3.5	Y 50	145.9	25.2	82.0
	Y 75	130.4	26.3	75.8
4.5	Y 50	126.7	23.3	72.2
	Y 75	110.9	24.3	69.8

reported in Figure 4, consistently to the literature on HSSDIs with high silicon content and slow solidification rates.[13–16]

Quality Assessment Procedure

The dislocation-density-related Voce constitutive equation[3,4] comes into

$$\sigma = \sigma_V + (\sigma_o - \sigma_V) \cdot \exp\left(-\varepsilon_p/\varepsilon_c\right) \quad \text{Eqn. 1}$$

where σ is the true flow stress, ε_p is the true plastic strain, σ_V is the saturation stress, ε_c is the characteristic transient strain that defines the rate with which σ_V is achieved and σ_o is the back-extrapolated stress to $\varepsilon_p = 0$. Even if σ_o is not the yield stress, it is quite close to it. To find the Voce parameters in Eqn. 1 from the experimental tensile flow curves to be modeled, the differential form of the Voce equation is used:

$$\frac{d\sigma}{d\varepsilon_p} = \frac{\sigma_V}{\varepsilon_c} - \frac{\sigma}{\varepsilon_c} = \Theta_o - \frac{\sigma}{\varepsilon_c} \quad \text{Eqn. 2}$$

where $d\sigma/d\varepsilon_p$ is the strain hardening rate and Θ_o the dislocation multiplication parameter. Θ_o is inversely related to the characteristic material length; so for, coarse microstructure with large characteristic size Θ_o is small or vice versa for finer microstructure with smaller characteristic size Θ_o decreases. Θ_o and ε_c are considered constants during straining. Through fitting Eqn. 2 to the linear regions at high stresses of the differential experimental data ($d\sigma/d\varepsilon_p$ vs. σ), the Voce parameters Θ_o and ε_c are found, and in turn σ_V (= $\varepsilon_c \times \Theta_o$). Details of the fitting procedure are reported in References [13].

In order to analyze quantitatively the effects of potential defects on the strain hardening behavior of samples of the same material, the plastic strain energy density (SED) at the uniform strain $\varepsilon_{u,p}$, hereafter called SED_U, has been proved to be a useful tool.[8] The uniform strain $\varepsilon_{u,p}$ is the strain where localized deformation in the form of necking occurs in tensile test. SED_U is the volumetric plastic strain energy (MJ/m^3) absorbed in the tensile sample until the uniform strain $\varepsilon_{u,p}$ and is defined as

$$SED_U = \int_0^{\varepsilon_{u,p}} \sigma(\varepsilon_p)\, d\varepsilon_p \qquad \text{Eqn. 3}$$

where $\sigma(\varepsilon_p)$ is the tensile flow curve and $\varepsilon_{u,p}$ according to Voce formalism is defined as

$$\varepsilon_{u,p} = \varepsilon_c \cdot \ln\left[\frac{\varepsilon_c + 1}{\varepsilon_c} \cdot \frac{\sigma_V - \sigma_o}{\sigma_V}\right] \qquad \text{Eqn. 4}$$

Failure in sound materials that are tensile tested occurs finally because of localized plastic deformation beyond necking, that is, $\varepsilon_p > \varepsilon_{u,p}$. However, if defects that are stress raisers are present in the materials, the flow stress needed to achieve failure may be reduced because it is occurring before necking, depending on the defect sizes and density. So the energy absorbed by the specimen during tensile testing is a potential assess of defects in materials, and the higher the defect sizes and density, the lower the absorbed energy. When the effects of defects on strain hardening are significant, a direct comparison between elongations to rupture according to the quality assessment procedure is meaningless.[8] So SED_U analysis could be a further tool for comparing the strain hardening behavior and integrity of GJS 400 produced through Y-blocks and heavy sections, and HSSDIs with 3.5 and 4.5 wt% silicon contents produced through different Y-blocks.

Results

GJS 400 Tensile Results

Y-Blocks GJS 400

The MAD for GJS 400 is reported in Figure 5, where the Voce data of GIS 400 produced through the four different Y-blocks lay on a specific region of the diagram along a specific line, identifying univocally the Y-blocks GJS 400. The intercept of the data best fitting line was positive (+ 2.06). In Figure 6 are reported the model flow curves (true stress–true strain) until the uniform strain $\varepsilon_{u,p}$ from three selected Y-blocks GJS 400 samples. With increasing Θ_o, the tensile and the yield strength of the material increase, that is, the saturation stress σ_V and the initial stress σ_o increase.

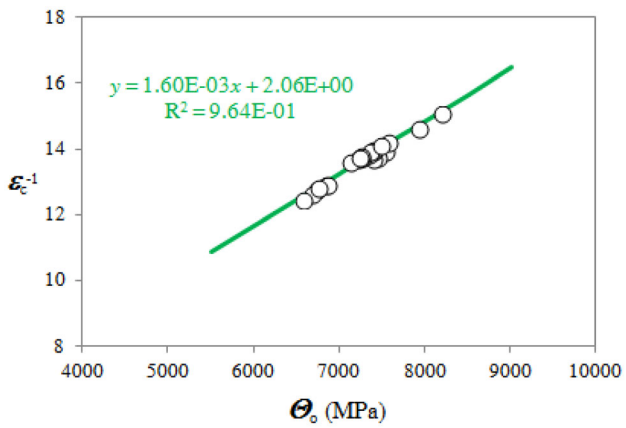

Figure 5. Matrix assessment diagram (MAD) for GJS 400 produced in three different Y- and Lynchburg-blocks.

It is important to bear in mind that in Figure 6 the true stress–true strain flow curves are models with strain values up to the uniform strains $\varepsilon_{u,p}$, regardless of the fact that these strains were actually achieved or not. Indeed, in GJS 400 produced through Y-blocks, the uniform strains (and so the necking) were always achieved, so the theoretical uniform strains $\varepsilon_{u,p}$ could be compared to the experimental ones, finding an underestimation of about − 7%. Hollomon equation was also fitted to the experimental flow curves to calculate the uniform strain according to Hollomon formalism, but the underestimation was of about − 20%. So the smaller average error suggested that the theoretical uniform strains $\varepsilon_{u,p}$ calculated through Voce formalism were more reliable, as already proved in Reference 5. The usefulness of this approach will be evident when the SED_U values versus the Voce parameters are considered.

Heavy Section GJS 400

The MAD for GJS 400 produced through heavy section is reported in Figure 7, where the GJS 400 data from the 14 different positions in the heavy section lay on a specific region of the diagram along a specific line, identifying univocally the tested material. The Voce analysis was performed up to ε_p = 0.03 of the experimental tensile flow curves, since the extensometers did not work beyond 0.03 during the tensile tests. In fact, reliable linear Voce behaviors in the strain range 0.01–0.03 (about 1–3% elongations) were found, while above 0.03 deviations from

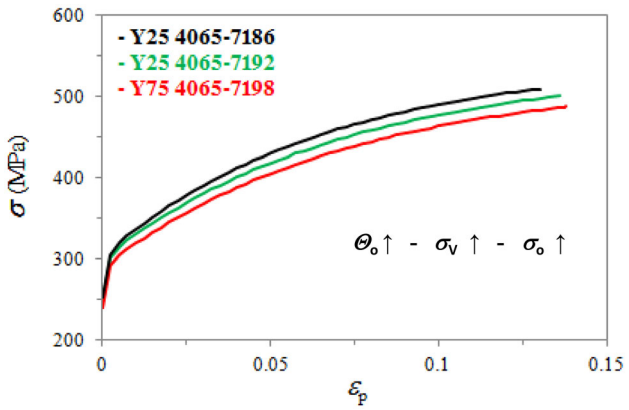

Figure 6. Selected model true stress–true strain flow curves of GJS 400 produced in four Y-blocks: With increasing Θ_o, the strength of DJS 400 (σ_V) and yield stress (σ_o) also increase.

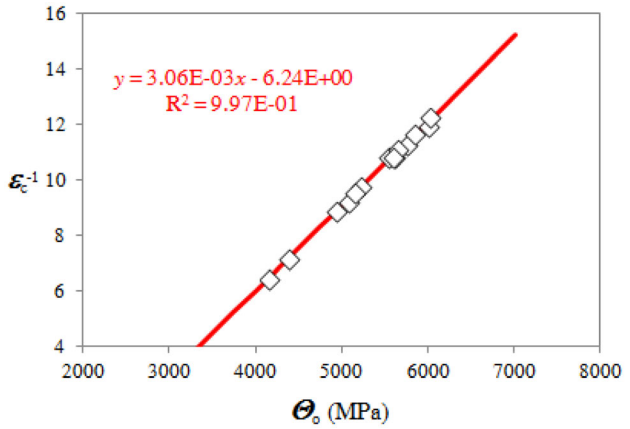

Figure 7. Matrix assessment diagram (MAD) for GJS 400 produced in heavy section.

linearity were originated because of the shift from strain control (below 0.03) to stroke control (beyond $\varepsilon_p = 0.03$).

It is noteworthy that in Figure 7 the intercept of the best fitting line of the heavy section GJS 400 data was negative (− 6.24), conversely to the results reported for the Y-blocks GJS 400. In Figure 8 are reported three selected model true stress–true strain flow curves until the uniform strain $\varepsilon_{u,p}$ from three selected positions in the heavy section. The flow curves are models with strain values up to the uniform strains $\varepsilon_{u,p}$, regardless of the fact that these strains were achieved or not. For instance, the real elongation to rupture of the sample D_Ext was 0.091, considerably lower than the uniform strain of 0.16 reported in Figure 6. Consistently to the negative intercept of the best linear fit (− 6.24) found in MAD, and to the relationship among the Voce parameters, that is, $\sigma_V = \varepsilon_c \times \Theta_o$, and differently to the plastic behavior found in the GJS 400 produced though Y-blocks, now with increasing Θ_o the strength of the material (σ_V) decreased significantly, while the initial σ_o was constant. Indeed, this tensile plastic behavior has been already reported in References 14 and 15 for DIs with silicon content lower than 3 wt% produced in heavy sections, where the authors reported that low nodularity and graphite degeneracy with chunky graphite that formed because of slow cooling rates decreased elongations to rupture and ultimate tensile strengths, without affecting yield strengths.

In Figures 6 and 8, model true stress–true strain flow curves up to the uniform strains (regardless of the fact that they were achieved or not) were considered, so they were representative of ideal plastic behavior. Defects and metallurgical discontinuities could reduce the real elongations to rupture, as indeed occurred in GJS 400 produced through heavy section. The differences in uniform elongations and heights between the Y-blocks (Figure 6) and heavy section (Figure 8) flow curves might be indicative of differences in chemical compositions and production routes, and further investigations should necessary to rationalize them.

HSSDI Tensile Results

3.5 wt% HSSDI

The MAD for 3.5 wt% HSSDI is reported in Figure 9. The Voce data lay on a specific region of the diagram along a specific best fitting line with positive intercept (+ 2.54). In Figure 10 are reported the model flow curves (true stress–true strain) until the uniform strain $\varepsilon_{u,p}$ of three selected samples. With increasing Θ_o, the tensile and the yield strengths of the material increase, that is, the saturation stress σ_V and the initial stress σ_o increase, consistently to the physical meaning of Voce equation. So in 3.5 wt% HSSDI the strain hardening behavior and the MAD analysis are consistent with the results of GJS 400 produced in Y-blocks reported in "Y-Blocks GJS 400" section. It is noteworthy that in 3.5 wt% HSSDI samples the uniform strains (and so the necking) were always achieved, so the

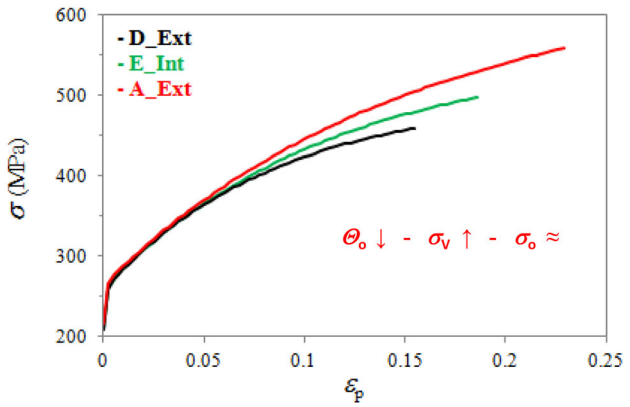

Figure 8. Selected model true stress–true strain flow curves of GJS 400 produced in heavy section: With increasing Θ_o, the strength of DJS 400 (σ_V) deceases, while the yield stress (σ_o) is constant.

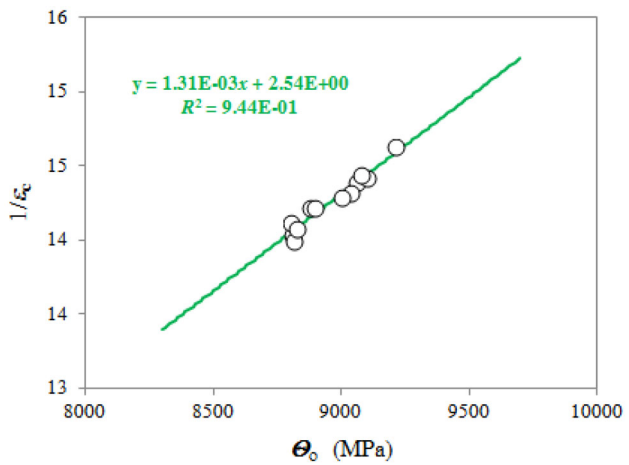

Figure 9. Matrix assessment diagram (MAD) for 3.5 wt% HSSDI produced in 50- and 75-mm Y-blocks.

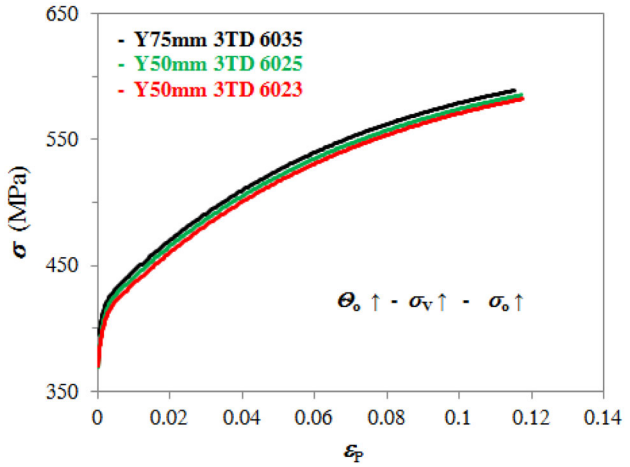

Figure 10. Model true stress–true strain flow curves of three selected 3.5 wt% HSSDI samples produced in 50- and 75-mm Y-block: With increasing Θ_o, the strength (σ_V) and yield stress (σ_o) also increase.

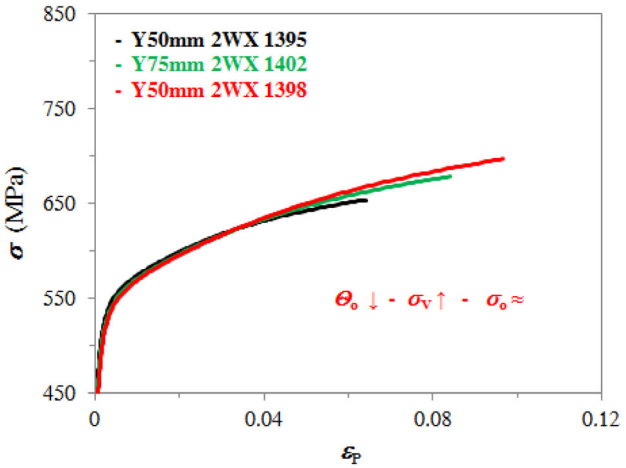

Figure 12. Model true stress–true strain flow curves of selected 4.5 wt% HSSDI produced in 50- and 75-mm Y-blocks: With increasing Θ_o, the strength (σ_V) deceases, while the yield stress (σ_o) is almost constant.

theoretical uniform strains $\varepsilon_{u,p}$ could be compared to the experimental ones, finding an excellent match with an underestimation of the experimental $\varepsilon_{u,p}$ of about − 0.02%.

4.5 wt% HSSDI

The MAD for 4.5 wt% HSSDI is reported in Figure 11. The Voce data lay on a specific region of the diagram along a specific best fitting line. However, the intercept of the best fitting line is negative (− 4.43). In Figure 12, the model flow curves (true stress–true strain) until the uniform strain $\varepsilon_{u,p}$ of selected samples are reported. Consistently to the considerations of the MAD results reported for GJS 400 produced in heavy section ("Heavy Section GJS 400" section), now with increasing Θ_o, the tensile strength of the material decreases, while the yield stress maintained constant, which is not consistent with the physical meaning of Voce equation. So in 4.5 wt% HSSDI the strain hardening behavior and the MAD analysis results are consistent with the results of GJS 400 produced in heavy section reported in "Heavy Section GJS 400" section.

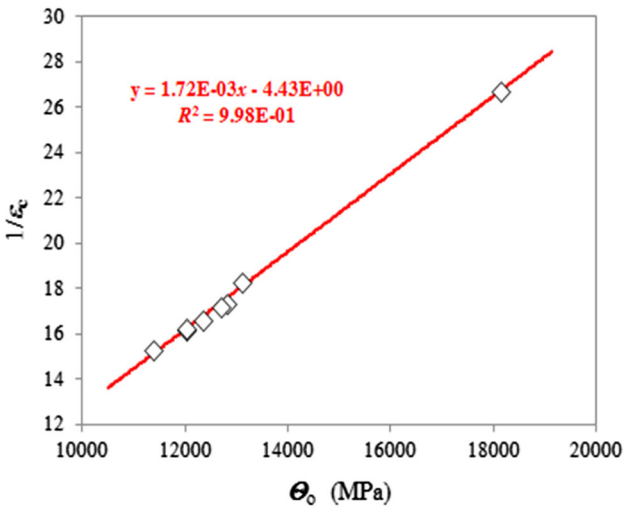

Figure 11. Matrix assessment diagram (MAD) for 4.5% HSSDI produced in 50- and 75-mm Y-blocks.

In Figure 12 are reported the model true stress–true strain flow curves until the uniform strain $\varepsilon_{u,p}$ of selected samples from Y-blocks 75 and 50 mm, for which the intercept of the best linear fit was negative (-4.43). With increasing Θ_o, the strength of the material decreased significantly, that is, the saturation stress σ_V, while the initial σ_o maintained constant. In References 13–16 decreased elongations to rupture and ultimate tensile strengths, without affecting yield strengths, have been reported for HSSDIs, where low nodularity and graphite degeneracy with chunky graphite formed because of high silicon content and slow cooling rates.

Discussion

All tensile strain hardening data of GJS 400 and HSSDIs lied on specific regions in the MAD, along specific lines, proving further that the MAD analysis is useful in DIs grade classification based on chemical composition and production route. However, two opposing plastic behaviors were highlighted in the MAD analysis, since the intercepts of the best fitting lines could indeed be positive or negative. Positive intercept meant that with increasing Θ_o the tensile and the yield strengths of the material increased. This behavior was found in the GJS 400 produced in Y-blocks and 3.5 wt% HSSDI, where nodularity was excellent. When the intercept of the best fitting line in MAD was negative, the tensile plastic behavior was opposite, since with increasing Θ_o the tensile strength decreased, while the yield strength was constant. This behavior was found in the

GJS 400 produced in heavy section and 4.5 wt% HSSDI, where nodularity deceased significantly.

Similar behavior of Figures 8 and 12 has been reported in aluminum castings that are well known to be highly defected,[21–25] suggesting further that the anomalous strain hardening behavior of the heavy section GJS 400 and the 4.5 wt% HSSIs could be also caused by defects. In Table 2, poor nodularity was reported in heavy section GJS 400, indicating some extent of graphite degeneracy that is evident in Figure 2. No detailed micrographs of chunky graphite are reported in Reference 18, even if the presence of chunky graphite has been widely reported for heavy section products.[9,10,19,20] In Table 3, also in 4.5 wt% HSSDI some graphite degeneracy was present with considerable nodularity decrease, and some chunky graphite is also reported in Figure 4. So, even if no correlation as reported in References 19 and 20 between the unusual plastic behavior and chunky graphite was possible, there was an evident connection between unusual plastic behavior and graphite degeneracy that is known to be detrimental for tensile mechanical properties. In fact, graphitic nodules with low spherical shape factor are defects, as they can present sharp features that can act like stress raisers, nucleating and propagating cracks. This causes reduction and variability of ductility and SED_U. However, it was noteworthy that even if the strain hardening should be significantly affected by defects, the Voce parameters of the heavy section GJS 400 in Figure 7 and HSSDIs in Figure 11 could lay on specific lines. So Θ_o and $1/\varepsilon_c$ were correlated also in materials where defects should be significant, and a random effect on strain hardening behavior should be expected. So the capability of the MAD to identify materials with potential metallurgical discontinuity and defects was evaluated.

The positive intercept (+ 2.06) of the best linear fit of the Y-blocks GJS 400 and (+ 2.54) of 3.5 wt% HSSDI were consistent with the physical interpretation of Voce equation, according to which the large Θ_o is correlated with finer microstructure,[3,4] resulting in stronger material with increasing yield and tensile strengths. Consistently to this interpretation, in Figures 6 and 10 the model tensile flow curves (true stress–true strain) with increasing Θ_o presented increasing σ_V and σ_o. The negative intercept (− 6.24) of the best linear fit of the heavy section GJS 400 and (− 4.42) of 4.5 wt% HSSDI resulted in an opposite plastic behavior. In fact, since the saturation stress σ_V is given by $\varepsilon_c \times \Theta_o$, negative intercept meant that higher Θ_o should have resulted in lower σ_V, which was in contrast to the physical meaning of Voce equation. Indeed, this behavior (increasing Θ_o, with decreasing σ_V and constant σ_o) has been often reported in aluminum castings where the sizes and density of defects are dramatically high. Interestingly, in the investigation reported in Reference 23 when the aluminum castings were hot isostatic pressed (HIP) to reduce the sizes and density of defects, the plastic behavior of the HIP aluminum samples became consistent with Figures 6 and 10 (increasing Θ_o, with increasing σ_V and σ_o), that is, consistent with the physical meaning of Voce equation.

The SED_U values of Y-blocks and heavy section GJS 400 versus Θ_o are reported in Figure 13, while from 3.5 and 4.5 wt% SED_U data are reported in Figure 14. The first evidence was that two different trends of the sets of data were present. The SED_U values from the Y-blocks GJS 400 and the 3.5 wt% HSSDI were independent on the Voce parameter Θ_o. The horizontal green line in Figure 13 was the SED_U mean value of GJS 400 produced in heavy section, namely 58.2 MJ/m^3 with an absolute mean variance of 0.7 MJ/m^3. The same behavior is reported in Figure 14 for 3.5 wt HSSDI, where the horizontal green line was the SED_U mean value of 3.5 wt% HSSDI, namely 60.6 MJ/m^3 with an absolute mean variance of 0.3 MJ/m^3. The same behavior SED_U versus Θ_o was found for IDI 800, where it was proved that strain hardening behavior was not affected by defects.[8] Conversely, in heavy section GJS 400 the SED_U values spanned from 57.7 to 102.5 MJ/m^3, resulting in a mean value of 70.5 MJ/m^3 with an absolute mean variance of 9.5 MJ/m^3. Also in 4.5 wt% HSSDI in Figure 14, the SED_U is significantly dependent on the Voce parameter Θ_o, varying from 39.2 to 61.2 MJ/m^3, resulting in a mean value of 55.4 MJ/m^3 with an absolute mean variance of 4.8 MJ/m^3. The same behavior SED_U versus Θ_o was reported for aluminum casting data.[8] So the heavy section data presented a high variability that was typical of the presence of large sizes and high density of defects, which is distinctive of heavy section DIs.[9–12,19,20] Degenerated graphite (low nodularity) as reported in Figure 2 for heavy section GJS 400 may have stress raisers that nucleate cracks, while proper spherical graphite (high nodularity) as reported in Figure 1 for Y-blocks GJS 400 is well known to be efficient obstacle to the crack propagation during tensile testing. The nodularity in Table 1 for Y-blocks GJS 400

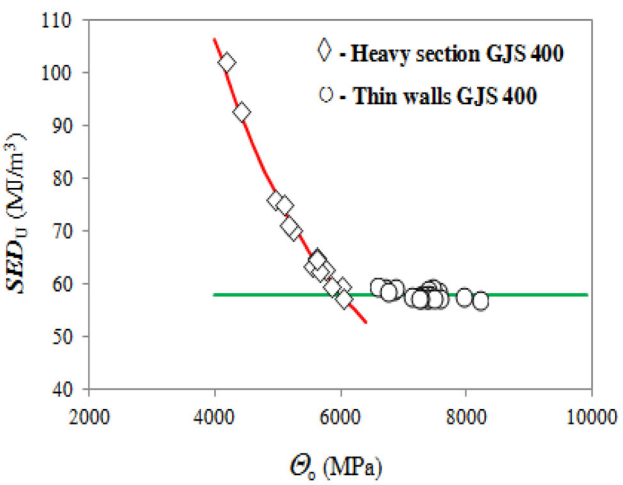

Figure 13. SED_U versus Θ_o of GJS 400 produced in Y-blocks and heavy section.

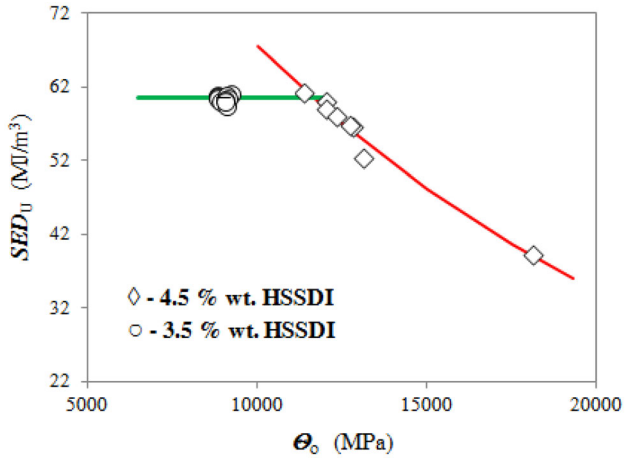

Figure 14. SED_U versus Θ_o of 3.5 and 4.5 wt% HSSDI produced in 50- and 75-mm Y-blocks.

was always higher than 83%, while in Table 2 for heavy section GJS 400 it was never higher than 76%, with a minimum of 57.6% for the position F_Ext in Table 2 with the microstructure reported in Figure 2. In Table 3, in HSSDI the nodularity for 3.5 wt% silicon content samples was always higher than 75%, while that for 4.5 wt% silicon content always was lower than 73%, with a minimum of 69.8% for the 75-mm Y-block. However, there was no direct correlation between microstructure parameters and plastic behaviors, so the nodularity results were only qualitative support to the different plastic behaviors.

The two different and opposite plastic behaviors could be explained qualitatively. Because of good nodularity, the nature and density of defects in the Y-blocks GJS 400 and 3.5 wt% HSSDI were below a significant threshold and did not affect the flow curve shapes, and in fact, the elongations to rupture were always beyond necking. The plastic behavior was consistent with the physical meaning of Voce equation. The sharp scatter of SED_U with no correlation with the Voce parameter Θ_o meant that the differences of plastic behaviors in the Y-blocks GJS 400 and 3.5 wt% HSSDI samples were caused by random microstructure features that affected the tensile flow curves (σ_V and σ_o), or even by contributions that could be related to measurement errors that were random by nature. Conversely, in the heavy section GJS 400 and 4.5 wt% HSSDI the SED_U and Θ_o were strongly related, since the nature and density of defects in the samples were probably so high that defects could contribute significantly to the plastic behaviors of the different samples, affecting the Voce parameters Θ_o and σ_V (and not σ_o).

The same anomalous plastic behavior here reported in GJS 400 heavy section and 4.5 wt% HSSDI has been reported also for aluminum castings that are well known to enclose defects with large sizes in high density.[21–25] So the anomalous plastic behavior for the DIs and aluminum castings, and in contrast to the physical interpretation of Voce equation, could be defined as *defect-driven plasticity*. Unfortunately, no direct indications of defects were found, and the low nodularity was just an indication of graphite degeneracy that could have produced stress raisers, so further investigation should be needed.

However, this investigation proved that the MAD could give useful information concerning not only the different chemical compositions and production routes of DIs, but also information about the presence of potential metallurgical defects by analyzing the intercept signs of the best lines fitting the Voce parameters in MAD. If the intercept is positive, the material is sound, while, if the intercept is negative, the material plastic behavior should be driven by defects that are relevant in sizes and density in the material. The more negative the intercept, the higher the size and density of the metallurgical discontinuities and defects. Deeper investigations on this interpretation are needed.

The correlations between Voce parameters in the matrix assessment diagram are indeed surprising. In the sound material where the plastic behavior is consistent with the physical interpretation of Voce equation,[3,4] Θ_o is the athermal component of strain hardening and $1/\varepsilon_c$ the dynamic recovery term that is thermal and describes the dislocation annihilation and formation of low-energy structures. To the author's knowledge, there is no apparent reason why Θ_o and $1/\varepsilon_c$ should be correlated in sound materials. So even more surprisingly was the correlation between Θ_o and $1/\varepsilon_c$ in the material that should be defected, since defects are expected to affect randomly the plastic behavior rather than describe a regular trend which could indicate the existence of a sort of *defect-driven plasticity*. These two surprising results should drive future investigations. However, so far some beneficial applications should be possible and here are reported considerations about those.

Conclusions

A new microstructure quality assessment procedure[3,4] is based on two diagrams: the matrix assessment diagram (MAD) capable of identifying unambiguously DIs produced with different silicon contents and various production routes, and the integrity assessment diagram (IAD) capable of identifying the presence of potential defects by comparing the elongations to rupture with the theoretical uniform elongations based on Voce formalism. The procedure is based on the fundamental assumption that the defects do not affect the strain hardening behavior of DIs. A comparison between the plastic behaviors of GJS 400 produced through Y-blocks and heavy sections, and between 3.5 and 4.5 wt% HSSDI, was reported, focusing on the capability of a material quality assessment procedure[3,4] to give indications of the integrity of the examined DIs even if strain hardening behaviors might be

significantly affected by metallurgical discontinuities and defects, like in GJS 400 produced in heavy section and in 4.5 wt% HSSDI. The following conclusions could be drawn:

- The matrix assessment diagram (MAD) could give useful information not only on the different chemical compositions and production routes of DIs, but also concerning the presence of potential metallurgical defects through analyzing the intercept signs of the best linear lines fitting the Voce parameters;
- The intercepts of the best linear fittings of the Voce parameters could be positive or negative: The positive intercepts reported for Y-blocks GJS 400 and 3.5 wt% HSSDI were consistent with the physical meaning of Voce equation (larger Voce parameter Θ_o, because of finer and stronger microstructure with larger σ_V), so the material was sound;
- If the intercept was negative like in the heavy section GJS 400 and 4.5 wt% silicon HSSDI, the material plastic behavior was in contrast to the physical interpretation of Voce equation, but was driven by defects (*defect-driven plasticity*) that were relevant in sizes and density in the material (larger Voce parameter Θ_o, weaker microstructure with lower σ_V); so, the material was defected;
- Strain energy density at uniform strain (SED_U) calculations were hardly scattered for the sound Y-blocks GJS 400 and 3.5 wt% silicon HSSDI with no relationship with Voce parameters, which was caused by random microstructure features that affected hardly the tensile flow curves, or even by contributions that could be associated with measurement errors that were random by nature;
- In the heavy section GJS 400 and 4.5 wt% silicon HSSDI, SED_U values and Voce parameter Θ_o were strongly related, since the nature and density of defects in the samples were so high that the defects contributed significantly to the plastic behaviors of the different samples, affecting σ_V (and not σ_o);
- SED_U analysis is also a useful tool to discriminate between sound and defected materials.

Acknowledgements

Mr. Davide Della Torre, Tullio Ranucci and Marcello Taloni are warmly thanked for their experimental support.

REFERENCES

1. F. Zanardi, F. Bonollo, N. Bonora, A. Ruggiero, G. Angella, A contribution to new material standards for ductile irons and austempered ductile irons. Int. J. Metalcast. **11**, 136–147 (2017). https://doi.org/10.1007/s40962-016-0095-6
2. Ductile iron data for design engineers/section III engineering data/part 1 tensile properties/relationships between tensile properties. www.ductile.org. Accessed 10 June 2019
3. U.F. Kocks, H. Mecking, Physics and phenomenology of strain hardening: the FCC case. Prog. Mater Sci. **48**, 171–273 (2003). https://doi.org/10.1016/S0079-6425(02)00003-8
4. Y. Estrin, Dislocation theory based constitutive modelling: foundations and applications. J. Mater. Process. Technol. **80–81**, 33–39 (1998). https://doi.org/10.1016/S0924-0136(98)00208-8
5. G. Angella, F. Zanardi, R. Donnini, On the significance to use dislocation-density-related constitutive equations to correlate strain hardening with microstructure of metallic alloys: the case of conventional and austempered ductile irons. J. Alloys Compd. **669**, 262–271 (2016). https://doi.org/10.1016/j.jallcom.2016.01.233
6. R. Donnini, F. Zanardi, F. Vettore, G. Angella, Evaluation of microstructure quality in ductile irons based on tensile behaviour analysis, in *Mat Sci Forum, 11th International Symposium on the Science and Processing of Cast Iron, SPCI-XI 2017; Jonkoping; Sweden*, vol. 925 (2018), pp. 342–349. https://doi.org/10.4028/www.scientific.net/MSF.925.342
7. G. Angella, F. Zanardi, Microstructure quality assessment of isothermed ductile irons through tensile tests, in *73rd World Foundry Congress Creative Foundry; WFC 2018—Proceedings* (2018), pp. 265–266. ISBN: 978-839043063-8
8. G. Angella, F. Zanardi, Validation of a new quality assessment procedure for ductile irons production based on strain hardening analysis. Metals **9**(8), 837 (2019). https://doi.org/10.3390/met9080837
9. J. Lacaze, L. Magnusson, J. Sertucha, Review of microstructural features of chunky graphite in ductile cast irons, in *2013 Keith Millis Symposium on Ductile Cast Iron, AFS, Nashville, USA* (2013), pp. 360–368. ISBN 978-0-87433-419-7
10. B. Bauer, I. Mihalic Pokopec, M. Petrič, P. Mrvar, Effect of Si and Ni addition on spheroidal morphology in heavy section spheroidal graphite iron parts, in *Mat Sci Forum, 11th International Symposium on the Science and Processing of Cast Iron, SPCI-XI 2017; Jonkoping; Sweden*, vol. 925 (2018), pp. 70–77. https://doi.org/10.4028/www.scientific.net/MSF.925.70
11. P. Ferro, A. Fabrizi, R. Cervo, C. Carollo, Effect of inoculants of containing rare earth metals and bismuth on microstructure and mechanical properties of heavy-sections near eutectic ductile cast iron castings. J. Mater. Process. Technol. **213**, 1601–1608 (2013). https://doi.org/10.1016/j.jmatprotec.2013.03.012

12. M. Benedetti, E. Torresani, V. Fontanari, D. Lusuardi, Fatigue and fracture resistance of heavy-section ferritic ductile cast iron. Metals **7**, 88–106 (2017). https://doi.org/10.3390/met7030088
13. P. Weiβ, J. Brachmann, A. Bührig-Polaczek, S.F. Fischer, Influence of nickel and cobalt on microstructure of silicon solution strengthened ductile iron. Mater. Sci. Technol. **31**, 1479–1485 (2015). https://doi.org/10.1179/1743284714Y.0000000735
14. U. de la Torre, A. Loizaga, J. Lacaze, J. Sertucha, As cast high silicon ductile irons with optimized mechanical properties and remarkable fatigue properties. Mater. Sci. Technol. **30**, 1425–1431 (2014). https://doi.org/10.1179/1743284713Y.0000000483
15. J. Sertucha, J. Lacaze, J. Serrallach, R. Suárez, F. Osuna, Effect of alloying on mechanical properties of as cast ferritic nodular cast irons. Mater. Sci. Technol. **28**, 184–191 (2012). https://doi.org/10.1179/1743284711Y.0000000014
16. U. de la Torre, J. Lacaze, J. Sertucha, Chunky graphite formation in ductile cast irons: effect of silicon, carbon and rare earths. Int. J. Mater. Res. (Form. Z. Metall.) **107**, 1041–1050 (2016). https://doi.org/10.3139/146.111434
17. G. Angella, R. Donnini, D. Ripamonti, M. Górny, F. Zanardi, The role of microstructure on tensile plastic behaviour of ductile iron GJS 400 produced through different rates—part II: tensile modeling. Metals **9**, 1019–1022 (2019). https://doi.org/10.3390/met9091019
18. G. Bertuzzi, G. Scarpa, Comparison of casting simulation results and experimental data in heavy section ductile iron production, in *International CAE Conference 2015, Pacengo del Garda (VR), Italy, 19–20 October* (2015), pp. 1–9
19. M. Gagné, D. Argo, Heavy section ductile iron castings—part I: structure and properties, in *International Conference on Advanced Casting Technology,* ed. by J. Easwaren (ASM International, 1987), pp. 231–244. ISBN: 0871702770
20. R. Källbom, K. Hamberg, L.E. Björkegren, Chunky-graphite—formation and influence on mechanical properties in ductile cast iron, in *Competent Design by Castings,* eds. by J. Samuelson, G. Marquis, J. Solin (2005). ISBN: 951.38.6299.2
21. M. Tiryakioğlu, J. Campbell, J.T. Staley, Evaluating structural integrity of Al–7%Si–Mg alloys via work hardening characteristics: I. Concept of target properties. Mater. Sci. Eng. A **368**, 205–211 (2004). https://doi.org/10.1016/j.msea.2003.10.311
22. M. Tiryakioğlu, J.T. Staley, J. Campbell, Evaluating structural integrity of Al–7%Si–Mg alloys via work hardening characteristics: II. A new quality index. Mater. Sci. Eng. A **368**, 231–238 (2004). https://doi.org/10.1016/j.msea.2003.10.310
23. M. Tiryakioğlu, N.D. Alexopoulos, J. Campbell, On the ductility potential of cast Al–Cu–Mg (206). Alloys Mater. Sci. Eng. A **506**, 23–26 (2009). https://doi.org/10.1016/j.msea.2008
24. M. Tiryakioğlu, J.T. Staley Jr., J. Campbell, The effect of structural integrity on the tensile deformation characteristics of A206-T71 alloy castings. Mater. Sci. Eng. A **487**, 383–387 (2008). https://doi.org/10.1016/j.msea.2007.11.005
25. M. Tiryakioğlu, J. Campbell, Quality index of aluminum casting alloys. Int. J. Metalcast. **8**, 39–42 (2014). https://doi.org/10.1007/BF03355589